



The response of excess ^{230}Th and extraterrestrial ^3He to sediment redistribution at the Blake Ridge, western North Atlantic

David McGee^{a,b,*}, Franco Marcantonio^c, Jerry F. McManus^{a,b}, Gisela Winckler^{a,b}

^a Lamont-Doherty Earth Observatory, 61 Route 9W, Palisades, NY 10964, United States

^b Department of Earth and Environmental Sciences, Columbia University, New York, NY 10025, United States

^c Department of Geology & Geophysics, Texas A&M University, MS 3115, College Station, TX 77843, United States

ARTICLE INFO

Article history:

Received 7 May 2010

Received in revised form 21 August 2010

Accepted 24 August 2010

Available online 25 September 2010

Editor: M.L. Delaney

Keywords:

thorium-230

helium-3

sediment focusing

mass accumulation rate

grain size

Blake Ridge

ABSTRACT

The constant-flux proxies excess ^{230}Th ($^{230}\text{Th}_{\text{xs}}$) and extraterrestrial ^3He ($^3\text{He}_{\text{ET}}$) are commonly used to calculate sedimentary mass accumulation rates and to quantify lateral advection of sediment at core sites. In settings with significant lateral input or removal of sediment, these calculations depend on the assumption that concentrations of $^{230}\text{Th}_{\text{xs}}$ and $^3\text{He}_{\text{ET}}$ are the same in both advected sediment and sediment falling through the water column above the core site. Sediment redistribution is known to fractionate grain sizes, preferentially transporting fine grains; though relatively few studies have examined the grain size distribution of $^{230}\text{Th}_{\text{xs}}$ and $^3\text{He}_{\text{ET}}$, presently available data indicate that both are concentrated in fine grains, suggesting that fractionation during advection may bias accumulation rate and lateral advection estimates based on these proxies. In this study, we evaluate the behavior of $^{230}\text{Th}_{\text{xs}}$ and $^3\text{He}_{\text{ET}}$ in Holocene and last glacial samples from two cores from the Blake Ridge, a drift deposit in the western North Atlantic. At the end of the last glacial period, both cores received large amounts of laterally transported sediment enriched in fine-grained material. We find that accumulation rates calculated by normalization to ^{230}Th and ^3He are internally consistent despite large spatial and temporal differences in sediment advection. Our analyses of grain size fractions indicate that ~70% of $^3\text{He}_{\text{ET}}$ -bearing grains are in the <20 μm fraction, with roughly equal amounts in the <4 and 4–20 μm fractions. $^{230}\text{Th}_{\text{xs}}$ is concentrated in <4- μm grains relative to 4- to 20- μm grains by approximately a factor of 2 in Holocene samples and by a much larger factor (averaging a factor of 10) in glacial samples. Despite these enrichments of both constant-flux proxies in fine particles, the fidelity of ^{230}Th - and ^3He -based accumulation rate estimates appears to be preserved even in settings with extreme sediment redistribution, perhaps due to the cohesive behavior of fine particles in marine settings.

© 2010 Elsevier B.V. All rights reserved.

1. Introduction

Paleoceanographic studies commonly rely upon reconstructions of past burial rates of calcium carbonate, opal, terrigenous material and other sedimentary constituents. These fluxes are calculated by multiplying the concentration of a given constituent by the sedimentary mass accumulation rate (MAR) and are thus dependent on the accuracy of MAR estimates.

Two methods are commonly used to derive sedimentary MARs. In the first, MARs are determined by dividing the dry mass of sediment between two horizons (the product of the dry bulk density and the

distance between the horizons) by the difference in age between the horizons. MARs estimated in this manner are hereafter referred to as age model MARs.

A second means of calculating MARs is provided by constant flux proxies (CFPs), sedimentary constituents that can be taken to have a known and constant flux to the seafloor. Here, MARs are determined by dividing the flux of a given CFP to the seafloor by the measured concentration of that CFP in the sediment. These CFP-normalized MARs differ from age model MARs in several important respects. First, while age model MARs reflect the combined effects of both vertical sediment inputs and lateral advection to and from the site, CFP-normalized MARs are interpreted as representing the preserved vertical rain rate. Differences between CFP-normalized MARs and age model MARs then provide estimates of the net effect of sediment redistribution at the site (i.e., the focusing factor; Suman and Bacon, 1989). This approach relies on the assumption that CFP concentrations are equal in sediment from the overlying water column and laterally advected sediments. Additionally, CFP-normalized MARs provide instantaneous MAR estimates at each sampled horizon, while age model MARs give average rates between dated horizons.

* Corresponding author. Lamont-Doherty Earth Observatory, 61 Route 9W, Palisades, NY 10964, United States. Tel.: +1 412 508 4644; fax: +1 845 365 8155.

E-mail addresses: dmcgee@ldeo.columbia.edu (D. McGee), marcantonio@tamu.edu (F. Marcantonio), jmcmanus@ldeo.columbia.edu (J.F. McManus), winckler@ldeo.columbia.edu (G. Winckler).

¹ Present address: Department of Geology and Geophysics, University of Minnesota, Minneapolis, MN 55455.

The two most widely used CFPs are unsupported (excess) ^{230}Th and extraterrestrial ^3He . ^{230}Th is produced in the water column by the decay of ^{234}U , which has constant salinity-normalized concentrations throughout the world's oceans due to the long residence time of U in seawater. As Th is efficiently scavenged by particles, lateral transport of ^{230}Th after its production is minimal (Anderson et al., 1983b; Henderson et al., 1999; Siddall et al., 2008), and the flux of scavenged ^{230}Th to the seafloor can reasonably be assumed to equal its known production rate in the water column above the core site (Bacon, 1984; Francois et al., 2004; Henderson and Anderson, 2003). Concentrations of scavenged ^{230}Th (hereafter $^{230}\text{Th}_{\text{xs}}$) are calculated by correcting total ^{230}Th concentrations for detrital ^{230}Th , ^{230}Th supported by authigenic U precipitated in sediments, and ^{230}Th decay in the time since sediment deposition.

Extraterrestrial ^3He ($^3\text{He}_{\text{ET}}$) is carried by interplanetary dust particles (IDPs), extraterrestrial grains small enough to avoid He loss during atmospheric entry heating. $^3\text{He}_{\text{ET}}$ values must be corrected for terrigenous ^3He using the $^3\text{He}/^4\text{He}$ ratio in the sediment and the $^3\text{He}/^4\text{He}$ ratios of the IDP and terrigenous end members, which differ by approximately 4 orders of magnitude. The flux of $^3\text{He}_{\text{ET}}$ has been approximately constant during the Quaternary (Brook et al., 2000; Marcantonio et al., 1995, 1996, 2001; Winckler and Fischer, 2006; Winckler et al., 2004).

Recently, inconsistencies between age model MARs and CFP-normalized MARs in studies of equatorial Pacific sediments have led some to question ^{230}Th - and ^3He -normalization (Broecker, 2008; Lyle et al., 2005; Paytan et al., 2004). Age model MARs suggest large changes in sediment accumulation in the equatorial Pacific over Late Quaternary glacial–interglacial cycles, while CFP-normalized MARs indicate roughly constant preserved vertical rain rates (Anderson et al., 2008; Higgins et al., 2002; Kienast et al., 2007; Loubere et al., 2004; Marcantonio et al., 2001; Paytan et al., 2004). Measurements of $^{230}\text{Th}_{\text{xs}}$ and $^3\text{He}_{\text{ET}}$ suggest that the age model MAR variations are driven either by glacial–interglacial changes in sediment redistribution or by systematic age model errors. Lyle et al. (2005) argue that sedimentary evidence does not support widespread sediment redistribution in the region and suggest that one explanation of the discrepancy is that $^{230}\text{Th}_{\text{xs}}$ is highly enriched in laterally advected clay-sized particles, biasing ^{230}Th -normalized MARs. According to this hypothesis, relatively minor advection of $^{230}\text{Th}_{\text{xs}}$ -enriched clays would lead to large increases in sedimentary $^{230}\text{Th}_{\text{xs}}$ concentrations without significant additions of mass. As a result, ^{230}Th -normalized MARs would underestimate vertical rain rates and overestimate sediment focusing during times of increased clay advection.

Existing data provide preliminary constraints on the grain size distribution of $^{230}\text{Th}_{\text{xs}}$ and $^3\text{He}_{\text{ET}}$. ^{230}Th adsorption is likely correlated with surface area, leading to elevated $^{230}\text{Th}_{\text{xs}}$ concentrations in fine particles (Francois et al., 2007). Consistent with this prediction, Anderson et al. (1983a) found that $^{230}\text{Th}_{\text{xs}}$ concentrations were enriched in suspended particles relative to sinking particles in Panama Basin samples by a factor of 1.5 to 3, while Thomson et al. (1993) found that $^{230}\text{Th}_{\text{xs}}$ concentrations were a factor of 2 higher in <5- μm grains than in 20- to 400- μm grains in carbonate-rich sediments from the northeast Atlantic. Recently, Kretschmer et al. (2010) conducted a systematic assessment of $^{230}\text{Th}_{\text{xs}}$ concentrations in different grain size fractions. In the two carbonate-rich samples analyzed, $^{230}\text{Th}_{\text{xs}}$ concentrations were a factor of 2–2.5 higher in the <2- μm fraction than in the 2- to 20- μm fraction, while in the two opal-rich sediment samples $^{230}\text{Th}_{\text{xs}}$ concentrations were a factor of 6–10.5 higher in the <2- μm fraction than in the 2- to 20- μm fraction. The study also documented robust relationships between surface area and $^{230}\text{Th}_{\text{xs}}$ concentrations, as predicted (Kretschmer et al., 2010).

For $^3\text{He}_{\text{ET}}$, measurements of a 1.5-kg sample of Antarctic ice found that >70% of $^3\text{He}_{\text{ET}}$ resided in the 5- to 10- μm fraction (Brook et al., 2009). A sample of 33 Ma North Pacific sediment suggested a broader distribution of $^3\text{He}_{\text{ET}}$ -bearing particles, with only 29% of $^3\text{He}_{\text{ET}}$ in the

<13- μm fraction and only slightly smaller proportions in the 13- to 37-, 37- to 53- and >53- μm fractions, but the inventory in the fine fraction in this study may be an underestimate due to flocculation of fine particles (Mukhopadhyay and Farley, 2006). Finally, a model of atmospheric entry heating suggests that approximately 70% of $^3\text{He}_{\text{ET}}$ should be found in 3- to 35- μm particles (Farley et al., 1997). Note that in considering the grain size distribution of each CFP, we focus on concentrations for $^{230}\text{Th}_{\text{xs}}$, as relative differences in $^{230}\text{Th}_{\text{xs}}$ concentrations should reflect differences in surface area to volume ratios between size fractions; for $^3\text{He}_{\text{ET}}$, the size distribution of which is determined by the size distribution of ^3He -retentive IDPs, we compare the proportion of the total $^3\text{He}_{\text{ET}}$ inventory found in each size fraction, as $^3\text{He}_{\text{ET}}$ concentrations will be influenced by the sediment supply in each size fraction.

These studies of grain size fractions indicate that both CFPs may be enriched in fine grains, suggesting some potential for size fractionation to compromise CFP-normalized estimates of MARs and lateral advection. In this study, we take a complementary approach by testing the response of $^{230}\text{Th}_{\text{xs}}$ and $^3\text{He}_{\text{ET}}$ to sediment advection in two cores from the Blake Ridge, a drift deposit lying in the path of the Western Boundary Undercurrent (WBUC) in the North Atlantic Ocean (Fig. 1). Cores KNR140-2 GGC39A and GGC40 are separated by only 10 km, and so should have approximately equal vertical rain rates. This assertion is supported by similar age model-based sand MARs at both sites throughout the last 20 kyr; as sand-sized particles are unlikely to be laterally transported, sand MARs can be used to estimate relative differences in local rain rates (Keigwin and Schlegel, 2002; Thomson et al., 1993). Age model MARs of bulk sediment at GGC39 are consistently higher than at GGC40, and age model MARs at both sites are much higher in the last glacial period than in the Holocene, dominantly reflecting spatially and temporally variable additions of laterally advected sediments (Fig. 2).

$^{230}\text{Th}_{\text{xs}}$ has been measured previously in two other Blake Ridge cores: 51GGC (1790 m) and CH88-11 (3337 m) (Gutjahr et al., 2008; Luo et al., 2001). Age model MARs suggest that, like the two cores in this study, CH88-11 experienced high rates of lateral advection during the last glacial period and deglaciation and much lower lateral advection in the Holocene. The shallower core 51GGC has experienced an opposite pattern, with minimal sediment advection during the last glacial period and much higher age model MARs during the Holocene (Gutjahr et al., 2008) (Fig. 2). Gutjahr et al. (2008) suggested that portions of Blake Ridge lying near the core of the WBUC should experience low deposition due to high current speeds, and they related the glacial–Holocene shift in depositional patterns to changes in the depth of the current. During the last glacial period, sortable silt data suggest that the core of the WBUC was between 2250 and 1750 m and that current speeds were low between 2500 and 4000 m, limiting deposition at 51GGC and allowing high deposition at CH88-11 and the two cores in this study. In the Holocene current speeds appear to have substantially increased between 3000 and 4000 m (Evans and Hall, 2008), a finding in agreement with observations that the modern WBUC core lies between 3500 and 4000 m on the Blake Ridge (Stahr and Sanford, 1999). This shift is thought to have limited deposition at CH11-88, GGC39 and GGC40 (all between 2900 and 3400 m water depth) and allowed for increased deposition at the shallower site 51GGC (Gutjahr et al., 2008).

The wide range of sediment advection experienced by GGC39 and GGC40, combined with the expectation that vertical rain rates should be equivalent at the two sites, provides a novel test of fractionation of $^{230}\text{Th}_{\text{xs}}$ and $^3\text{He}_{\text{ET}}$ during lateral transport. This study complements previous studies of ^{230}Th in drift sites (Francois et al., 1993; Kienast et al., 2007; Thomson et al., 1993, 2006) and comprises the first study of $^3\text{He}_{\text{ET}}$ in a drift site. We test for fractionation by evaluating the internal consistency of ^{230}Th - and ^3He -normalized MARs and by comparing average $^3\text{He}_{\text{ET}}/^{230}\text{Th}_{\text{xs}}$ ratios in the two cores in both the Holocene and the glacial. In so doing, we place limits on the degree to which CFP-normalized MARs may be compromised by lateral sediment advection.

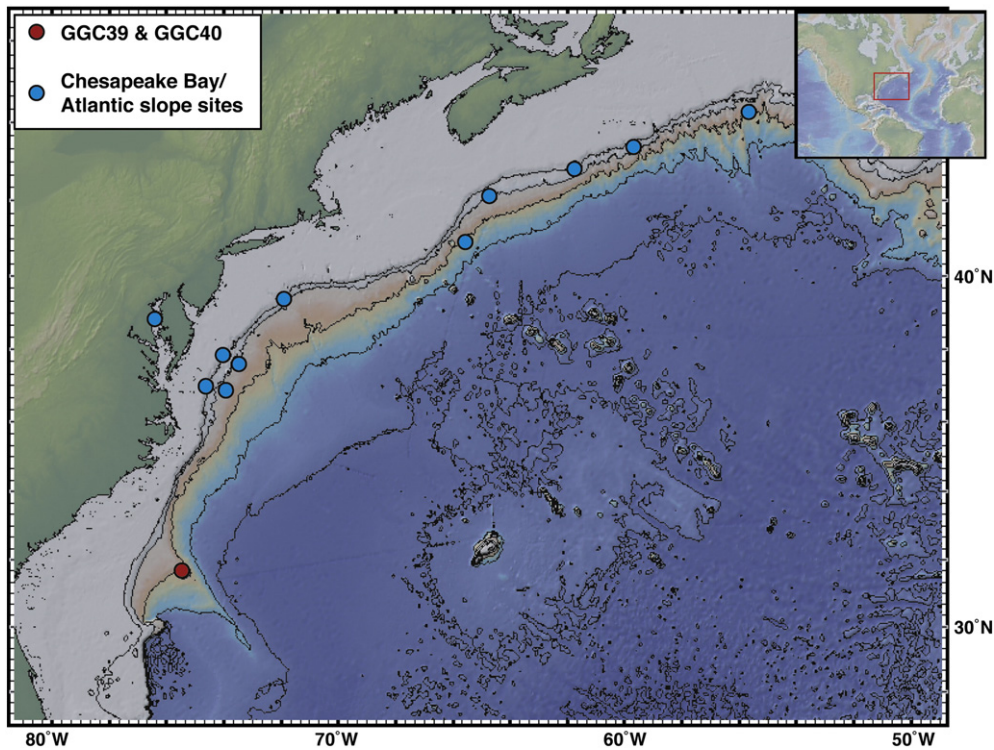


Fig. 1. Map showing locations of cores sampled for this study. Locations for all cores are listed in Table 1.

We also evaluate concentrations of $^{230}\text{Th}_{\text{xs}}$ and $^3\text{He}_{\text{ET}}$ in different grain size fractions of the sediment to determine the extent to which each is concentrated in the fine fraction of these drift sediments.

2. Methods

2.1. Core sites

Samples were taken from two cores separated by approximately 10 km along the Blake Ridge: KNR140-2 GGC39A ($31^{\circ}40'\text{N}$, $75^{\circ}25'\text{W}$; 2975 m) and KNR140-2 GGC40 ($31^{\circ}43'\text{N}$, $75^{\circ}28'\text{W}$; 2924 m). U-Th analyses were performed on samples throughout the last 19 ka in each core at 10-cm intervals. The He analyses were performed on samples from Holocene (coretop to 6–9 ka) and late glacial (18–19 ka) time slices in each core; and U-Th and He analyses of grain size fractions were performed on Holocene and late glacial samples from GGC39.

The age model for GGC39 is based on 11 ^{14}C dates younger than 20 ka, while that for GGC40 is based on one coretop ^{14}C date and correlations with carbonate and magnetic susceptibility data from GGC39 at 6 tie points between 8.5 and 18.3 ka (Keigwin and Schlegel, 2002). The age model for GGC40 is extrapolated between 180 and 200 cm (>18.3 ka) using accumulation rates from the last dated interval (130–170 cm). In an effort to identify the He isotopic composition of the detrital sediments deposited at these sites, we also analyzed the He isotopic composition of 10 samples from coretops north of the Blake Ridge along the western Atlantic continental slope and 2 samples from the Chesapeake Bay (Fig. 1; Table 1).

In the Holocene time slice, age model MARs are a factor of 2 higher at GGC39 than at GGC40 (average 7.6 vs. 3.8 $\text{g cm}^{-2} \text{kyr}^{-1}$) (Fig. 2). Age model MARs at both sites are higher in the late glacial time slice (hereafter, glacial): values reach 37 $\text{g cm}^{-2} \text{kyr}^{-1}$ at GGC40, while at GGC39 age model MARs have values of >70 $\text{g cm}^{-2} \text{kyr}^{-1}$ for extended periods of the late glacial with a short-lived peak to 149 $\text{g cm}^{-2} \text{kyr}^{-1}$ (Keigwin and Schlegel, 2002). Errors in calibrated radiocarbon ages and

age model tie points cause substantial uncertainty in glacial and deglacial age model MAR values, particularly where tie points are close together (as in the peak to 149 $\text{g cm}^{-2} \text{kyr}^{-1}$ at GGC39, for which a 1-sigma confidence interval spans from 35 to ∞ $\text{g cm}^{-2} \text{kyr}^{-1}$). Though individual age model MAR values may have large errors, the overall pattern of higher glacial age model MARs is robust: the 1-sigma confidence interval for the age model MAR for the period between ^{14}C dates at 235 cm and 391 cm in GGC39 is 59 to 136 $\text{g cm}^{-2} \text{kyr}^{-1}$.

Assuming that vertical rain rates are the same at both sites, differences between age model MARs between the sites must reflect differences in lateral sediment advection. Contributions from lateral advection (focusing factors) are commonly estimated by comparing sedimentary $^{230}\text{Th}_{\text{xs}}$ and $^3\text{He}_{\text{ET}}$ inventories to predicted vertical inputs of each tracer over a dated sediment interval; however, as the fidelity of $^{230}\text{Th}_{\text{xs}}$ and $^3\text{He}_{\text{ET}}$ is being tested in the present study, we make independent estimates of lateral advection rates. If we conservatively assume Holocene deposition at GGC40 (3.8 $\text{g cm}^{-2} \text{kyr}^{-1}$) reflects local rain rates, laterally advected sediments then account for 50% of Holocene sediments at GGC39 (7.6 $\text{g cm}^{-2} \text{kyr}^{-1}$) (i.e., the Holocene focusing factor in GGC39 is 2).

Turning to the glacial time slice, the high age model MARs at both sites likely reflect a combination of higher vertical rain rates and higher lateral advection to the sites. To estimate the relative importance of these two factors, we use age model-derived sand accumulation rates (sand MARs). Because sand-sized particles are unlikely to be laterally transported large distances, changes in sand MAR provide an indication of the relative Holocene–glacial difference in rain rates. Sand MARs are only a factor of 2–2.5 higher in the glacial than in the Holocene at both sites (Keigwin and Schlegel, 2002). Multiplying this difference by the Holocene age model MAR at GGC40 (3.8 $\text{g cm}^{-2} \text{kyr}^{-1}$) to estimate local rain rates in the glacial, we find that higher rain rates account for only a small portion of the increase in age model MARs (i.e., rain rates were a maximum of 7.5 – 10 $\text{g cm}^{-2} \text{kyr}^{-1}$, and were likely less). As the remainder of the increase must come from an increase in deposition of laterally advected sediments, laterally advected sediments likely

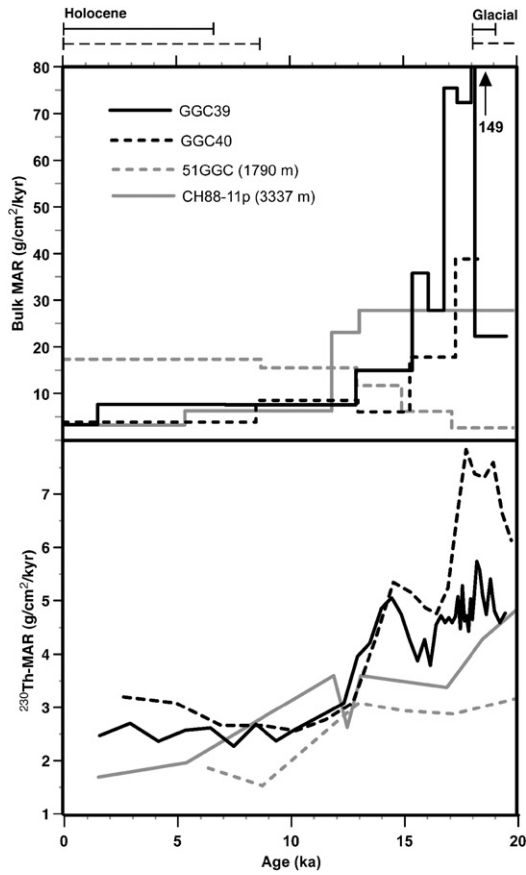


Fig. 2. (Top) Age model MARs at GGC39 and GGC40 calculated using published age control points and dry bulk densities (black) (Keigwin and Schlegel, 2002) and age model MARs from previously studied sites 51GGC and CH88-11 (grey) (Gutjahr et al., 2008; Luo et al., 2001; MARs for these two cores assume constant dry bulk density of 0.7 g/cc) and (bottom) MARs calculated by $^{230}\text{Th}_{\text{ex}}$ -normalization. Note the different scales in the two plots. Bars at the top of the figure represent portions of GGC39 and GGC40 sampled for He analysis and measurement of grain size fractions in this study; the solid line represents GGC39 and the dashed line represents GGC40. Age model MARs were not calculated for GGC40 below 170 cm (18.3 ka), the location of the final age control point in the core. The maximum age in the glacial time slice in this core is thus approximate.

account for >70% of sediments at GGC40 and up to >90% of sediments at GGC39 in the glacial (i.e., focusing factors of ~4 and up to >10, respectively).

Table 1

Locations and depths of cores used in this study.

Blake Ridge cores	Latitude (°N)	Longitude (°W)	Depth (m)
KNR140-2 GGC39A	31.67	75.42	2975
KNR140-2 GGC40	31.72	75.47	2924
Atlantic margin cores			
VM27-12	44.28	55.65	2814
VM17-169	43.38	59.65	2138
VM17-171	42.85	61.73	1061
RC6-4	42.13	64.70	1977
VM7-69	40.93	65.55	2974
KZ81-7	37.87	74.00	1678
KZ81-14	37.65	73.47	2400
V15-210	37.02	74.60	672
RC17-1	36.90	73.93	2537
Chesapeake Bay cores			
MD99-2209	38.89	76.39	26
MD03-2661	38.89	76.40	26

2.2. Helium isotope data

Because carbonate contains negligible He (Marcantonio et al., 1995), carbonate was dissolved in samples from GGC39 and GGC40 prior to helium isotope analysis to improve counting statistics by concentrating the He-retentive portion of the sediments. Approximately 1 g of bulk sediment was leached in 200 mL of 0.5 N acetic acid solution until no reaction was observed. We then rinsed the remaining sample twice in distilled water, freeze-dried it, and prepared Al foil-wrapped balls containing ~0.3 g sediment each. Due to their relatively low carbonate contents, we did not dissolve carbonate from Atlantic slope and Chesapeake Bay sediments prior to analysis.

Sample balls were placed in a molybdenum crucible under vacuum and heated to ~1300 °C. A liquid nitrogen-cooled charcoal trap and an SAES getter purified the sample gas prior to its capture in a cryotrap at ~14 K. The trap was heated to 45 K to release He for isotopic analysis using a MAP 215–50 noble gas mass spectrometer. ^4He concentrations and $^3\text{He}/^4\text{He}$ ratios were calibrated using 0.2–2.0 cc air standards and a secondary Murdering Mudspot standard for low-He samples. Hot blanks contained $<1 \times 10^{-10}$ cc STP ^4He and $<1 \times 10^{-15}$ cc STP ^3He . Blanks were negligible for ^4He in all samples, were <2% for ^3He in bulk samples, and were <5% for ^3He in size fraction samples.

Analytical precision was typically better than 1% for ^4He and 3% for ^3He . Errors reported in Supplementary Table 1 reflect analytical errors, blank corrections, and the average error of the standard calibration. Replicates were run for 11 samples to monitor reproducibility, as this is the primary limit on the precision of our He data. For reasons thought to relate to variations in sampling a discrete number of IDPs, ^3He concentrations vary by between 1% and 79% in our replicates, with an average reproducibility of 36%. For 3 samples with the largest difference between replicates, we measured a third replicate and identified outliers using the Chauvenet criterion (Long and Rippeteau, 1974), which defines outliers as having a probability $<0.5/n$, where n is the number of replicates. For each of the 3 samples, one replicate was removed from the data set. ^4He concentrations were less variable, with an average reproducibility of 6%. Farley et al. (1997) suggest that sediment samples representing small time-area products (calculated as aliquot mass divided by age model MAR) will have poorer ^3He reproducibility due to increased IDP dilution. This formulation does not account for addition of IDPs through sediment advection, however, and so reproducibility does not correlate with time-area product in our samples (not shown).

Helium in our samples represents a binary mixture of terrigenous and extraterrestrial He. $^3\text{He}_{\text{ET}}$ concentrations are determined from measured ^3He concentrations ($[^3\text{He}_{\text{meas}}]$) and $^3\text{He}/^4\text{He}$ ratios ($^3\text{He}/^4\text{He}_{\text{meas}}$) using the isotopic compositions of the terrigenous and extraterrestrial (IDP) end members:

$$[^3\text{He}_{\text{ET}}] = [^3\text{He}_{\text{meas}}] \left(\frac{1 - \frac{^3\text{He}/^4\text{He}_{\text{TERR}}}{^3\text{He}/^4\text{He}_{\text{meas}}}}{1 - \frac{^3\text{He}/^4\text{He}_{\text{TERR}}}{^3\text{He}/^4\text{He}_{\text{IDP}}}} \right) \quad (1)$$

(Marcantonio et al., 1995) where $^3\text{He}/^4\text{He}_{\text{TERR}}$, the $^3\text{He}/^4\text{He}$ ratio of the terrigenous end member, is here taken to be 1.0×10^{-8} (see explanation in Section 3.2) and $^3\text{He}/^4\text{He}_{\text{IDP}}$, the $^3\text{He}/^4\text{He}$ ratio of IDPs, is 2.4×10^{-4} (Nier and Schlutter, 1990).

$^3\text{He}_{\text{ET}}$ -normalized MARs (^3He -normalized MARs) are then calculated assuming a constant flux of $^3\text{He}_{\text{ET}}$:

$$^3\text{He} - \text{normalized MAR} = f_{\text{He}} / [^3\text{He}_{\text{ET}}] \quad (2)$$

where f_{He} , the $^3\text{He}_{\text{ET}}$ flux, is $8 \pm 2 \times 10^{-13}$ cc STP $\text{cm}^{-2} \text{kyr}^{-1}$ (Brook et al., 2000, 2009; Marcantonio et al., 1995, 1996, 2001) and $[^3\text{He}_{\text{ET}}]$ is the $^3\text{He}_{\text{ET}}$ concentration in cc STP/g.

2.3. Uranium and thorium isotope data

Dried and homogenized sediment samples weighing 0.3–0.4 g were spiked with ^{229}Th and digested in a combination of HF, HNO_3 , and HClO_4 . After U and Th isotopes were extracted by iron oxy-hydroxide coprecipitation, an aliquot of the resulting solution was spiked with ^{236}U and was used for determination of ^{238}U and ^{232}Th concentrations. Th in the remaining solution was purified using ion exchange chromatography and analyzed for ^{230}Th and ^{229}Th (McManus et al., 2004; Mollenhauer et al., 2006). Analyses were performed on a Finnegan MAT Element I single collector, sector field, inductively coupled plasma mass spectrometer at Woods Hole Oceanographic Institution using the methods of Choi et al. (2001). Counting statistics and replicate analyses indicate that errors on ^{230}Th concentrations are $\leq 5\%$ (Supplementary Table 2).

^{230}Th concentrations were corrected for detrital ^{230}Th using measured ^{232}Th concentrations and a detrital $^{238}\text{U}/^{232}\text{Th}$ activity ratio of 0.6 (Anderson et al., 1994; Henderson and Anderson, 2003; McManus et al., 1998, 2004). Sensitivity to the detrital activity ratio is discussed in Section 3.3. Resulting values were corrected for radioactive decay using existing age models (Keigwin and Schlegel, 2002) and a half-life for ^{230}Th of 75.7 kyr (Cheng et al., 2000). A correction was also made for ingrowth of ^{230}Th from authigenic ^{234}U by determining authigenic U concentrations from ^{238}U in excess of the assumed detrital $^{238}\text{U}/^{232}\text{Th}$ activity ratio, assuming a $^{234}\text{U}/^{238}\text{U}$ activity ratio of 1.146, and assuming authigenic deposition at the seafloor.

^{230}Th -normalized MARs were calculated by dividing the water column production rate of ^{230}Th by the measured $^{230}\text{Th}_{\text{xs}}$ concentrations (in dpm g^{-1}):

$$^{230}\text{Th} - \text{normalized MAR} = \beta \times z / [^{230}\text{Th}_{\text{xs}}], \quad (3)$$

where β is the ^{230}Th production rate ($0.0268 \text{ dpm m}^{-3} \text{ yr}^{-1}$ at a salinity of 35, based on the U concentration and $^{234}\text{U}/^{238}\text{U}$ ratio of seawater determined by Robinson et al., 2004) and z is the water depth (m) (for more information, see Francois et al., 2004).

2.4. Carbonate data

CaCO_3 abundance data for all samples from GGC39 and most samples from GGC40 are from Schlegel (1998). Carbonate percentages for the three deepest samples from GGC40 and for Atlantic slope sediments were measured by coulometry at LDEO.

2.5. Grain size separation

Grain size separations were performed on three samples from the Holocene and glacial time slices in each core, for a total of 12 samples, though only samples from GGC39 were analyzed for helium and thorium isotopes (Table 2). Sediment samples weighing $\sim 15 \text{ g}$ were separated into $>63\text{-}\mu\text{m}$ and 20- to $63\text{-}\mu\text{m}$ fractions by wet sieving. Settling was used to separate the 4- to $20\text{-}\mu\text{m}$ and the $<4\text{-}\mu\text{m}$ fractions.

Table 2

Average weight proportions in each size fraction after grain size separation. Data represent the mean of three samples per time slice per core.

	$>63 \mu\text{m}$	20–63 μm	4–20 μm	$<4 \mu\text{m}$
<i>GGC39</i>				
Holocene average	$5.8 \pm 0.2\%$	$6.1 \pm 1.5\%$	$45.8 \pm 1.1\%$	$42.3 \pm 1.4\%$
Glacial average	$3.4 \pm 1.7\%$	$5.5 \pm 2.3\%$	$48.7 \pm 4.4\%$	$41.6 \pm 6.1\%$
<i>GGC40</i>				
Holocene average	$8.3 \pm 4.2\%$	$8.3 \pm 1.3\%$	$44.2 \pm 2.2\%$	$39.2 \pm 4.0\%$
Glacial average	$6.2 \pm 0.5\%$	$11.4 \pm 2.5\%$	$45.3 \pm 3.5\%$	$37.2 \pm 5.9\%$

Samples of the $<20\text{-}\mu\text{m}$ fraction were placed in a graduated cylinder in a dilute (0.04%) sodium hexametaphosphate solution at 20°C , stirred, and left to settle. A settling velocity of 0.00087 cm/s for $4 \mu\text{m}$ particles, calculated using the modifications of Wadell (1932, 1934) to account for non-spherical particles, was used to calculate the settling time. A density of 2.6 g/cc was measured for a subset of samples using a pycnometer at LDEO and was used in calculating the settling velocity. We note that if spherical particles are assumed, the operationally defined diameter of the fine fraction is $3.1 \mu\text{m}$. After all $>4\text{-}\mu\text{m}$ grains were calculated to be in the lower 40% of the graduated cylinder, the top 60% of the solution was siphoned into a second container. Additional solution was then added to the remaining sample to return it to its original volume, and the procedure was repeated 2 additional times. Addition of sodium hexametaphosphate does not produce measurable effects on $^{230}\text{Th}_{\text{xs}}$ or $^3\text{He}_{\text{ET}}$ concentrations in sediments (J.F.M., unpublished data; A. Torfstein, pers. comm. 2009).

3. Results

3.1. Helium isotope data

Helium isotope ratios and concentrations were measured on a total of 27 samples and 14 replicates from GGC39 and GGC40. $^3\text{He}/^4\text{He}$ ratios span approximately an order of magnitude, from 1.7 to $14 (\times 10^{-8})$, with lower ratios in glacial samples (Fig. 3A; Supplementary Table 1). ^3He concentrations in the non-carbonate fraction ($\text{NC}[^3\text{He}]$) vary with $^3\text{He}/^4\text{He}$ ratios; as shown in Fig. 3A, a plot of the reciprocals of $^3\text{He}/^4\text{He}$ and $\text{NC}[^3\text{He}]$ produces linear arrays consistent with mixing between IDP and terrigenous end members. Glacial samples from GGC39 form an array distinct from other samples on this plot, with low ^3He concentrations relative to $^3\text{He}/^4\text{He}$ ratios.

$^3\text{He}/^4\text{He}$ ratios in sediments from 10 Atlantic slope cores and 2 Chesapeake Bay sites were approximately the same as in glacial samples from Blake Ridge; only 3 samples had lower $^3\text{He}/^4\text{He}$ than the minimum values in GGC39 and GGC40. The Atlantic slope samples define a separate linear array on the mixing plot due to their relatively high He concentrations, while the Chesapeake Bay samples lie approximately along the mixing trend for Blake Ridge samples.

3.2. Extraterrestrial ^3He deconvolution and MAR calculation

In order to deconvolve terrigenous ^3He from extraterrestrial ^3He using Eq. (1), we use a value of 1.0×10^{-8} for $^3\text{He}/^4\text{He}_{\text{TERR}}$. A previous study of North Atlantic sediments used a higher value for $^3\text{He}/^4\text{He}_{\text{TERR}}$ (2.0×10^{-8}) based on average production ratios for the upper continental crust and measurements of Chinese loess (Farley and Patterson, 1995), but low $^3\text{He}/^4\text{He}$ ratios in glacial GGC40 samples indicate that $^3\text{He}/^4\text{He}_{\text{TERR}}$ must be $<1.6 \times 10^{-8}$. $^3\text{He}/^4\text{He}$ data from Atlantic margin and Chesapeake Bay sediments representing potential terrigenous sources reach 1.4×10^{-8} , while data from grain size fractions are as low as 1.05×10^{-8} . Analyses of the non-magnetic fraction of sediments (thought to contain dominantly terrigenous He) from the central North Atlantic suggest a $^3\text{He}/^4\text{He}_{\text{TERR}}$ of $0.5 \pm 0.3 \times 10^{-8}$ (Fourre, 2004), indistinguishable from the $^3\text{He}/^4\text{He}$ ratio in ice-rafted detrital sediments from a Heinrich Event layer (0.588×10^{-8} ; Marcantonio et al., 1998). These central North Atlantic and Heinrich layer results likely represent an unrealistically low value for $^3\text{He}/^4\text{He}_{\text{TERR}}$ in Blake Ridge sediments, as they include high inputs of Labrador Sea sediments from exceptionally old (presumably ^4He -rich) terranes. Taken together, these results suggest that our chosen $^3\text{He}/^4\text{He}_{\text{TERR}}$ of 1.0×10^{-8} is generally reasonable.

We find that $^3\text{He}_{\text{ET}}$ accounts for 78–91% of total ^3He in Holocene samples and 37–82% of total ^3He in glacial samples. Average $^3\text{He}_{\text{ET}}$ -normalized MARs in both cores are a factor of 2–3 higher in the glacial than in the Holocene, and values agree between the two cores in both time periods (Fig. 4). ^3He -normalized MARs vary by a factor of 3–5

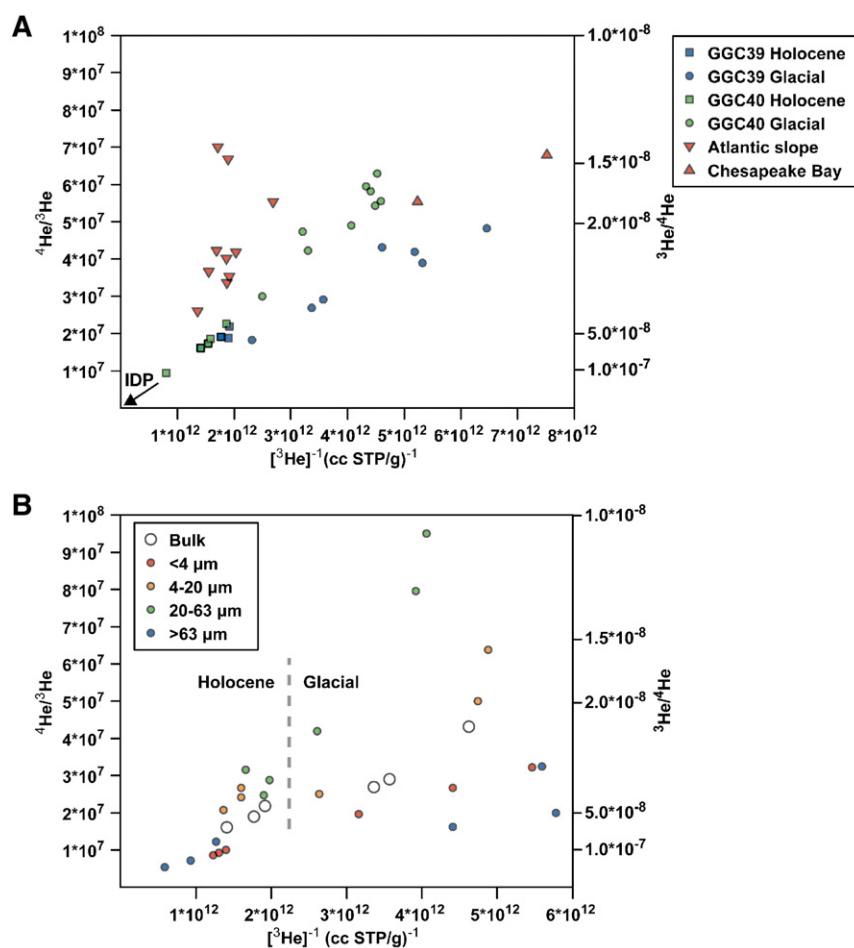


Fig. 3. $^4\text{He}/^3\text{He}$ ratios vs. the reciprocal of the ^3He concentration in the non-carbonate fraction of the sediment for (A) bulk samples in GGC39 and GGC40 and (B) grain size fractions in GGC39. Linear arrays reflect mixing between IDP (lower left) and terrigenous (upper right) end members. In (A), Holocene samples from both GGC39 and GGC40 and glacial samples from GGC40 form a single array, while glacial GGC39 samples and samples from Atlantic slope cores form separate subparallel arrays indicating terrigenous end members with slightly different compositions. ^3He concentrations in Chesapeake Bay samples are for bulk sediment due to a lack of carbonate data for these samples.

between individual samples during the glacial (Supplementary Table 1), likely due to poor reproducibility resulting from the dilution of a finite number of ^3He -bearing IDPs by large amounts of detrital sediments.

$^3\text{He}_{\text{ET}}$ inventories in the sediments are greater than the predicted influx in all core sections, exceeding supply by factors of 1.3 and 2.6 in the Holocene sections of GGC40 and GGC39, respectively, and by factors of 3.0 and 13.0 in the glacial sections; these factors correspond to the ^3He -based estimates of the ratio of total sediments to vertical rain, often referred to as focusing factors (Suman and Bacon, 1989). Inventories were only compared to supply for sediments down to 170 cm in GGC40, as the age model is not constrained below this level.

Calculated $^3\text{He}_{\text{ET}}$ values are sensitive to the chosen $^3\text{He}/^4\text{He}_{\text{TERR}}$, particularly in 5 glacial samples in GGC40 with $^3\text{He}/^4\text{He} < 2.0 \times 10^{-8}$. As a sensitivity test, we tested values of $^3\text{He}/^4\text{He}_{\text{TERR}}$ ranging from 0.5×10^{-8} to 1.3×10^{-8} . Holocene ^3He -normalized MARs vary by $\leq 10\%$ as a result of these changes in $^3\text{He}/^4\text{He}_{\text{TERR}}$. Glacial values are more sensitive; setting $^3\text{He}/^4\text{He}_{\text{TERR}}$ to 0.5×10^{-8} decreases glacial ^3He -normalized MARs by 25% and 37% in GGC39 and GGC40, respectively, while using a value of 1.3×10^{-8} increases glacial ^3He -normalized MARs by 26% and 62%. The means of these modified glacial ^3He -normalized MARs are not significantly different from the original mean values in either core.

3.3. Uranium and thorium isotope data

Concentrations of $^{230}\text{Th}_{\text{xs}}$ are a factor of 2–3 higher in Holocene sediments than in glacial sediments. Accordingly, ^{230}Th -normalized

MARs are a factor of 2–3 higher during the glacial than in the Holocene in both cores. ^{230}Th -normalized MARs are largely consistent between the two cores throughout the last 19 ka, with the exception of the late glacial and portions of the Holocene, when ^{230}Th -normalized MARs are significantly (up to ~40%) higher at GGC40 than at GGC39 (Fig. 2).

Glacial $^{230}\text{Th}_{\text{xs}}$ values are sensitive to the detrital $^{238}\text{U}/^{232}\text{Th}$ ratio used to correct for terrigenous ^{230}Th . Measurements of $^{238}\text{U}/^{232}\text{Th}$ ratios in surface sediments sampled by box cores from the Mid-Atlantic Bight, which should preserve the sediment–water interface and thus have negligible authigenic U in coretop sediments, suggest that the activity ratio in local terrigenous sediments is 0.60 ± 0.04 (Anderson et al., 1994). Using the high and low ends of this range, we find that average Holocene ^{230}Th -normalized MARs change by only 2%, while glacial ^{230}Th -normalized MARs in GGC39 and GGC40 change by 7% and 11% respectively.

Inventories of sedimentary $^{230}\text{Th}_{\text{xs}}$ exceed $^{230}\text{Th}_{\text{xs}}$ production in the local water column in each core section, with ratios of total $^{230}\text{Th}_{\text{xs}}$ to $^{230}\text{Th}_{\text{xs}}$ production (^{230}Th -based focusing factors) similar to ^3He -based focusing factors. The $^{230}\text{Th}_{\text{xs}}$ inventory exceeds production by factors of 1.5 and 2.6 in the Holocene in GGC40 and GGC39, respectively, and by factors of 3.0 and 16.3 in the glacial.

Sedimentary $^{238}\text{U}/^{232}\text{Th}$ activity ratios in both cores are higher than the assumed detrital activity ratio, averaging 1.3–1.4 in the Holocene and 0.74–0.76 in the glacial. These elevated ratios likely indicate the presence of authigenic U. Higher authigenic U concentrations in the Holocene (average 1.0–1.3 dpm/g) than in the glacial (average 0.4 dpm/g) may reflect increased dilution of authigenic uranium by laterally transported

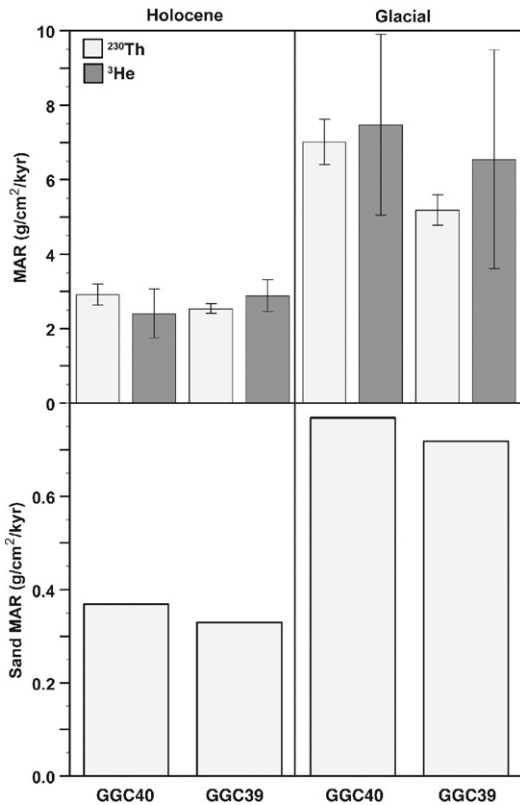


Fig. 4. (Top) Average MARs calculated by normalization to $^{230}\text{Th}_{\text{XS}}$ (light grey) and $^3\text{He}_{\text{ET}}$ (dark grey) for Holocene and glacial samples from GGC39 and GGC40. Time slices from the two cores are arranged in order of increasing sediment advection from left to right. Error bars show the standard error of the mean. (Bottom) Average sand MARs in each time slice calculated by multiplying average sand percentages by the age model MARs in each core section (Keigwin and Schlegel, 2002). Sand MARs are taken to represent a relative measure of the local sediment rain rate. The Holocene–glacial difference in sand MARs matches that in ^{230}Th - and ^3He -normalized MARs.

detrital sediments during the glacial; glacial and Holocene ^{230}Th -normalized burial rates for authigenic U are approximately the same at both sites.

3.4. Grain size fraction data

The proportional weight of each grain size fraction is shown in Table 2. Sand (>63 μm) percentages agree well with values measured by Keigwin and Schlegel (2002). Increases in age model MARs, which correspond to increases in advected sediments in these cores, result in dilution of coarser sediments; in both time periods the >63- μm and the 20- to 63- μm grain size fractions account for higher proportions of sediments at GGC40, the site with less advection, than at GGC39, and at both sites sand percentages are lower in the glacial than in the Holocene. There is very little difference in the proportion of <4 μm and 4–20 μm sediments between the two sites, as these fractions make up >80% of total sediments in all samples.

U-Th measurements were performed on a subset of the <4- μm and 4- to 20- μm samples from GGC39. Using the proportional weight of size fractions and $^{230}\text{Th}_{\text{XS}}$ concentrations in size fractions and bulk sediments, we were then able to calculate the $^{230}\text{Th}_{\text{XS}}$ concentrations in coarser size fractions required to achieve mass balance. In the Holocene, $^{230}\text{Th}_{\text{XS}}$ concentrations in the <4- μm fraction are on average a factor of 2 higher than concentrations in the 4- to 20- μm fraction or calculated concentrations for the total >4- μm fraction of the sediments (Fig. 5A; Table 3). In glacial sediments, the relative $^{230}\text{Th}_{\text{XS}}$ enrichment in the fine fraction is much greater: average $^{230}\text{Th}_{\text{XS}}$ concentrations in the fine fraction are only slightly lower than

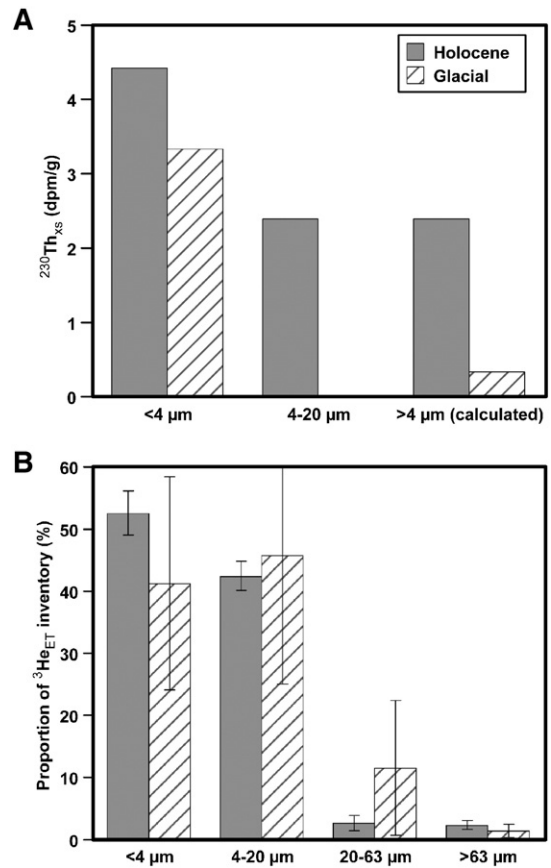


Fig. 5. (A) Concentrations of $^{230}\text{Th}_{\text{XS}}$ in grain size fractions of Holocene and glacial samples from GGC39. Concentrations in the >4- μm fraction of the sediment were calculated using concentrations in <4 μm fractions and bulk sediments and the proportion of <4- μm grains in the sediment. No 4–20 μm samples were analyzed for glacial sediments. $^{230}\text{Th}_{\text{XS}}$ is elevated in the <4- μm fraction relative to >4- μm grains by a factor of 1.8 in the Holocene and a factor of 10 in the glacial. (B) Proportions of $^3\text{He}_{\text{ET}}$ in size fractions of GGC39 sediments. More than 90% of $^3\text{He}_{\text{ET}}$ is in <20- μm grains, with roughly equal inventories in the <4- μm and the 4- to 20- μm fractions.

in Holocene sediments, but the lower bulk $^{230}\text{Th}_{\text{XS}}$ concentrations lead to very low (0–0.6 dpm/g) calculated $^{230}\text{Th}_{\text{XS}}$ concentrations in >4- μm grains. The causes for the increased enrichment of $^{230}\text{Th}_{\text{XS}}$ in the fine fraction in glacial samples are not known, and further investigation is required to determine whether this Holocene–glacial difference relates to the increased sediment redistribution in the glacial.

Her data indicate that the isotopic composition of the terrigenous end member changes with grain size (Fig. 3B); the <4- and >63- μm fractions tend to have lower ^4He concentrations and higher $^3\text{He}/^4\text{He}$ than the two intermediate fractions, raising the possibility that different $^3\text{He}/^4\text{He}_{\text{TERR}}$ values should be used when calculating $^3\text{He}_{\text{ET}}$ concentrations in each size fraction. We tested the sensitivity of $^3\text{He}_{\text{ET}}$ concentrations in each size fraction to the chosen $^3\text{He}/^4\text{He}_{\text{TERR}}$ by (a) using a constant $^3\text{He}/^4\text{He}_{\text{TERR}}$ of 1.0×10^{-8} (the same value used for the bulk data) and (b) using a value of 2.0×10^{-8} for the <4- and >63- μm fractions and 1.0×10^{-8} for the 4- to 20- and 20- to 63- μm fractions. Our reported results use scenario a; using scenario b, the proportion of $^3\text{He}_{\text{ET}}$ in <4- μm grains in glacial samples falls by 10% and $^3\text{He}_{\text{ET}}$ proportions rise in coarser size fractions, but the changes do not affect our findings.

Because $^3\text{He}_{\text{ET}}$ concentrations are determined in part by the supply of detrital and carbonate sediments in each size fraction (both of which dilute $^3\text{He}_{\text{ET}}$), we instead focus on the proportion of the total inventory of $^3\text{He}_{\text{ET}}$ in each size fraction. Inventories are calculated by multiplying the $^3\text{He}_{\text{ET}}$ concentration in each grain size fraction by the abundance of that grain size fraction in bulk sediment. We find that in both Holocene and glacial samples, >90% of $^3\text{He}_{\text{ET}}$ is found in the <20- μm fraction,

Table 3

U and Th isotope data for grain size fractions from GGC39. Data from glacial-aged horizons are shaded. The final column contains $^{230}\text{Th}_{\text{xs}}$ concentrations calculated for the >4- μm fraction of the sediments based on <4 μm and bulk data.

Size fraction	Depth (cm)	^{238}U (dpm g^{-1})	\pm	^{232}Th (dpm g^{-1})	\pm	^{230}Th (dpm g^{-1})	\pm	$^{230}\text{Th}_{\text{xs}}$ (dpm g^{-1})	Calculated $^{230}\text{Th}_{\text{xs}}$ for >4 μm fraction (dpm g^{-1})
< 4 μm	10-11	1.48	0.039	1.88	0.042	5.88	0.08	4.84	2.2
	30-31	2.44	0.049	1.83	0.036	4.83	0.03	3.87	3.0
	50-51	2.5	0.057	1.96	0.035	5.51	0.20	4.58	2.0
	360-361	2.17	0.041	3.23	0.058	5.38	0.10	4.05	0.4
	390-391	2.32	0.059	2.41	0.051	4.1	0.12	3.14	0.0
	420-421	1.97	0.062	2.56	0.089	3.92	0.09	2.83	0.6
4–20 μm	10-11	1.55	0.033	1.56	0.032	3.66	0.16	2.18	
	30-31	2.12	0.056	1.48	0.035	3.41	0.23	2.62	

with slightly higher inventories in the <4- μm fraction compared to the 4- to 20- μm fraction (Fig. 5B; Table 4).

When the He size fraction data are combined with the fractional weight of each size fraction, the grain size data reproduce bulk ^3He and ^4He concentrations with average errors of 18% and 6%, respectively. These values are similar to our reproducibility for each isotope on bulk replicate samples.

4. Discussion

4.1. Mixing between terrigenous and extraterrestrial ^3He

The sensitivity of $^3\text{He}_{\text{ET}}$ concentrations to $^3\text{He}/^4\text{He}_{\text{TERR}}$ led us to further investigate mixing relationships between terrigenous and IDP ^3He . Data from Holocene samples from both cores and from glacial GGC40 samples lie along a single mixing trend between IDP and terrigenous end members (Fig. 3A). Glacial samples from GGC39 define a subparallel array suggesting a distinct terrigenous end

member with higher $^3\text{He}/^4\text{He}$. Our size fraction measurements (Fig. 3B) show that the <4- μm fraction plots to the same side of the main bulk sample array as do the glacial GGC39 bulk values. This finding suggests to us that the GGC39 glacial samples define a separate array because they are enriched in low- ^4He , high- $^3\text{He}/^4\text{He}$ fine detrital material due to lateral advection. As our grain size fraction weights do not show a large increase in the proportion of <4 μm material in glacial GGC39 sediments (Table 2), we suggest that the 4- to 20- μm fraction in these sediments contains a greater proportion of finer grains within this size range than the 4- to 20- μm fractions of the other sediments.

In order to better characterize the terrigenous end member, we also measured the helium isotopic composition of 2 samples from the Chesapeake Bay and 10 samples from the Atlantic slope representing potential sources of terrigenous sediments delivered to Blake Ridge (Biscaye and Anderson, 1994; Heezen et al., 1966; Stahr and Sanford, 1999). Only the samples from the Chesapeake Bay plotted along the mixing lines defined by data from GGC39 and GGC40; all Atlantic

Table 4

He isotope data for grain size fractions from GGC39. Concentrations are expressed relative to sediment prior to carbonate removal. Loss on leaching value reflects weight change after 0.5 N acetic acid leach and is an approximation of the sample's carbonate content. Data from glacial-aged horizons are shaded.

Size fraction	Depth (cm)	Loss on leaching	^3He (cc STP g^{-1}) ($\times 10^{-13}$)	\pm	^4He (cc STP g^{-1}) ($\times 10^{-6}$)	\pm	$^3\text{He}/^4\text{He}$ ($\times 10^{-8}$)	\pm	$^3\text{He}_{\text{ET}}$ (cc STP g^{-1}) ($\times 10^{-13}$)
<4 μm	10-11	42%	4.75	0.07	4.09	0.03	11.64	0.16	4.35
	30-31	43%	4.09	0.11	4.09	0.03	10.00	0.26	3.68
	50-51	42%	4.46	0.09	4.13	0.03	10.81	0.20	4.05
	360-361	15%	1.93	0.09	5.14	0.04	3.75	0.18	1.41
	390-391 (replicate)	14%	1.62	0.05	5.13	0.03	3.16	0.09	1.11
	420-421	14%	1.53	0.04	5.01	0.03	3.06	0.09	1.03
4–20 μm	10-11	40%	2.71	0.11	5.30	0.04	5.10	0.20	2.18
	30-31	40%	3.76	0.12	9.08	0.11	4.14	0.12	2.85
	30-31	43%	3.57	0.10	9.54	0.06	3.75	0.10	2.62
	50-51	38%	4.54	0.09	9.41	0.06	4.82	0.09	3.60
	360-361	16%	1.73	0.04	11.05	0.09	1.57	0.04	0.63
	390-391 (replicate)	19%	1.55	0.05	8.99	0.06	1.72	0.05	0.65
20–63 μm	420-421	13%	1.88	0.09	8.27	0.05	2.28	0.10	1.06
	10-11	57%	3.28	0.10	8.24	0.05	3.98	0.12	2.46
	30-31	64%	2.26	0.10	5.59	0.05	4.05	0.18	1.70
	30-31	64%	1.39	0.04	5.81	0.04	2.38	0.06	0.80
	50-51 (replicate)	60%	1.79	0.07	5.80	0.06	3.09	0.12	1.21
	420-421	22%	2.20	0.12	5.72	0.04	3.85	0.21	1.63
>63 μm	360-361	21%	1.94	0.04	18.48	0.20	1.05	0.02	0.09
	390-391	29%	1.81	0.16	14.38	0.10	1.26	0.11	0.37
	420-421	22%	4.69	0.08	14.82	0.15	3.16	0.05	3.20
	10-11	88%	1.29	0.05	0.92	0.04	13.94	0.23	1.19
	30-31	88%	0.98	0.04	1.19	0.02	8.19	0.31	0.86
	50-51	88%	2.07	0.04	1.12	0.01	18.55	0.32	1.96
>63 μm	360-361	56%	0.79	0.02	2.58	0.02	3.08	0.06	0.54
	390-391	72%	0.63	0.05	1.03	0.06	6.16	0.29	0.53
	420-421	76%	0.41	0.03	0.82	0.01	5.00	0.37	0.33

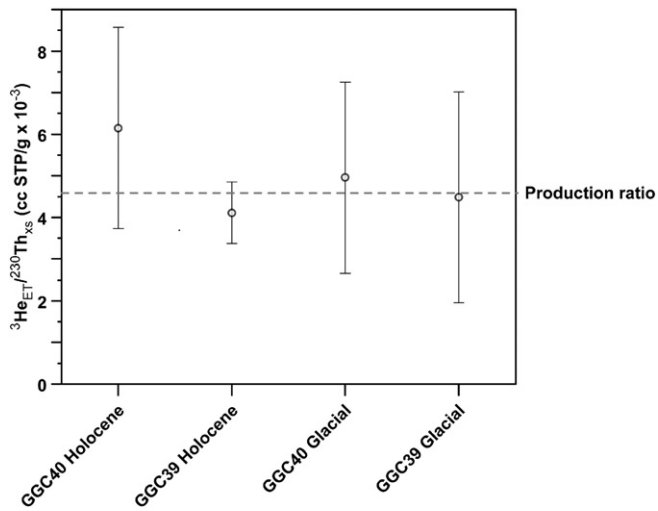


Fig. 6. Average ratios of ${}^3\text{He}_{\text{ET}}/{}^{230}\text{Th}_{\text{XS}}$ in Holocene and glacial samples from GGC39 and GGC40, with time slices arranged in order of increasing sediment advection from left to right. Errors are calculated using the standard errors of the mean ${}^3\text{He}_{\text{ET}}$ and ${}^{230}\text{Th}_{\text{XS}}$ concentrations for each time slice. The dashed line shows the ratio of the global ${}^3\text{He}_{\text{ET}}$ flux to the production rate of ${}^{230}\text{Th}_{\text{XS}}$ in the water column above our core sites. None of the observed ratios differs significantly from the production ratio, suggesting that lateral sediment advection does not fractionate ${}^{230}\text{Th}_{\text{XS}}$ from ${}^3\text{He}_{\text{ET}}$. We neglect the slight difference in the production ratio between the two sites (0.1×10^{-3} cc STP g^{-1}) that results from their different depths.

slope sediments had He concentrations that were higher than Blake Ridge sediments with similar ${}^3\text{He}/{}^4\text{He}$ ratios (Fig. 3A). This difference could suggest that Blake Ridge detrital material originates in or near the Chesapeake Bay. Alternatively, the difference between the Chesapeake and Atlantic slope samples could result from grain size differences, with the Atlantic slope array possibly reflecting the removal of low- ${}^4\text{He}$ fine material by bottom currents.

The low ${}^4\text{He}$ concentrations and high ${}^3\text{He}/{}^4\text{He}$ ratios of the $>63\text{-}\mu\text{m}$ fraction in GGC39 may indicate that this material has a different provenance than finer sediments (Fig. 3B). As sand-sized particles are unlikely to be laterally transported, these particles presumably have a local source while finer particles are dominantly advected. Low ${}^4\text{He}$ concentrations in the $<4\text{-}\mu\text{m}$ fraction relative to the 4- to 20- and 20- to 63- μm fractions are less likely to reflect a provenance difference and may instead result from ${}^4\text{He}$ diffusion and recoil loss from fine particles (Solomon et al., 1996; Tolstikhin et al., 1996) and from the presumed higher prevalence of low-He clay minerals in this fraction (Mamyrin and Tolstikhin, 1984).

4.2. Fractionation between ${}^3\text{He}_{\text{ET}}$ and ${}^{230}\text{Th}_{\text{XS}}$ during lateral advection

If ${}^3\text{He}_{\text{ET}}$ were to accumulate at these sites at the average global rate of 8×10^{-13} cc STP cm^{-2} kyr^{-1} (Brook et al., 2000; Marcantonio et al., 1996) and ${}^{230}\text{Th}_{\text{XS}}$ were to accumulate at its production rate in the overlying water column, sediments should have a ${}^3\text{He}_{\text{ET}}/{}^{230}\text{Th}_{\text{XS}}$ ratio of 4.6×10^{-3} cc STP g^{-1} . We note that there is $\sim 25\%$ uncertainty in this estimate due to uncertainties in the ${}^3\text{He}_{\text{ET}}$ flux and that the expected ratio is $\sim 2\%$ higher at GGC40 due to its shallower depth (and hence lower ${}^{230}\text{Th}_{\text{XS}}$ production rate in overlying waters).

Observed ${}^3\text{He}_{\text{ET}}/{}^{230}\text{Th}_{\text{XS}}$ ratios in Holocene and glacial samples from GGC39 and GGC40 are not significantly different from the predicted production ratio, providing no evidence for a relationship between sediment redistribution and fractionation of ${}^3\text{He}_{\text{ET}}$ from ${}^{230}\text{Th}_{\text{XS}}$ (Fig. 6). In particular, despite lateral sediment inputs comprising up to $>90\%$ of total sediments at GGC39 in the glacial

period, ${}^3\text{He}_{\text{ET}}/{}^{230}\text{Th}_{\text{XS}}$ ratios are not substantially different from the production ratio. Our results complement those of Fourre (2004), who found no evidence for ${}^3\text{He}_{\text{ET}}/{}^{230}\text{Th}_{\text{XS}}$ fractionation in a core from the central North Atlantic that had experienced winnowing.

Besides indicating that grain-size fractionation during lateral transport does not significantly separate ${}^3\text{He}_{\text{ET}}$ from ${}^{230}\text{Th}_{\text{XS}}$, these results also indicate that other potential biases caused by sediment redistribution have not affected ${}^{230}\text{Th}_{\text{XS}}$ concentrations. As pointed out by Francois et al. (1990), shallow shelf sediments and old sediments are initially depleted in ${}^{230}\text{Th}_{\text{XS}}$ with respect to locally derived sediments at a deep drift site, causing advection of these sediments to bias ${}^{230}\text{Th}$ -normalized MARs if sufficient equilibration with dissolved water column ${}^{230}\text{Th}$ does not occur in transit. Also, laterally advected sediments tend to be enriched in aluminosilicates relative to carbonate (Thomson et al., 2006); ${}^{230}\text{Th}_{\text{XS}}$ may thus be fractionated if it preferentially adsorbs to either particle class. As ${}^3\text{He}_{\text{ET}}$ concentrations should not be affected by water depth, sediment age or lithology, the consistency of ${}^3\text{He}_{\text{ET}}/{}^{230}\text{Th}_{\text{XS}}$ ratios suggests that these processes do not significantly affect ${}^{230}\text{Th}$ -normalized MARs in our samples. These findings corroborate and extend the conclusions of Francois et al. (1993) and Thomson et al. (1993, 2006) that advected sediments equilibrate with water column ${}^{230}\text{Th}_{\text{XS}}$ concentrations near their depositional sites and the finding by Chase et al. (2002) that lithology does not strongly affect ${}^{230}\text{Th}_{\text{XS}}$ concentrations.

4.3. Evaluation of ${}^{230}\text{Th}$ - and ${}^3\text{He}$ -normalized MARs

Though age model MARs at GGC39 have consistently been higher than those at GGC40 due to sediment advection, MARs normalized to constant flux proxies should “see through” this difference in sediment redistribution and produce MARs that approximate the preserved vertical sediment flux. CFP-normalized MARs should be nearly equal at the two sites, as it is unlikely that the vertical sediment flux differs substantially over a distance of only ~ 10 km.

In the Holocene, ${}^{230}\text{Th}$ - and ${}^3\text{He}$ -normalized MARs are consistent both with each other and between sites despite the fact that lateral advection causes age model MARs to be a factor of 2 higher at GGC39 than at GGC40 (Fig. 4). Our record of ${}^{230}\text{Th}$ -normalized MARs through the last 19 kyr demonstrates that values are consistent between the two sites and with two other Blake Ridge sites for most of this period, again despite large differences in age model MARs and thus in lateral sediment advection (Fig. 2) (Gutjahr et al., 2008; Luo et al., 2001). In the glacial time slice, when both cores, and in particular GGC39, have extremely high age model MARs (37 g cm^{-2} kyr^{-1} at GGC40 and up to >70 g cm^{-2} kyr^{-1} at GGC39), ${}^{230}\text{Th}$ - and ${}^3\text{He}$ -normalized MARs are consistent with each other within error, and ${}^3\text{He}$ -normalized MARs agree between the two sites (Fig. 4). Glacial ${}^{230}\text{Th}$ -normalized MARs at GGC40 are significantly (40%) higher than at GGC39 and at CH88-11 at a similar depth, for reasons that are at present unclear.

The difference in ${}^{230}\text{Th}$ -normalized MARs between the two sites during the glacial time slice may reflect additions of ${}^{230}\text{Th}_{\text{XS}}$ -rich fines at GGC39 and/or removal of ${}^{230}\text{Th}_{\text{XS}}$ -rich sediments from GGC40 during this period of extremely active sediment redistribution. A difference in sediment deposition at the two sites in the late glacial is supported by He isotope data; the He isotope mixing plot (Fig. 3A) shows that glacial GGC39 sediments diverge from glacial GGC40 sediments in the direction of $<4\text{-}\mu\text{m}$ material (Fig. 3B). Grain size data fail to show a large difference between the two sites during the glacial time slice: the $<4\text{-}\mu\text{m}$ grain size separates comprise 40% of glacial sediments at GGC40 and 43% at GGC39 (Table 2). This slight difference is not able to explain ${}^{230}\text{Th}_{\text{XS}}$ concentrations almost 40% higher at GGC39 during the glacial time slice, but the grain size data may underestimate the difference due to incomplete recovery of the $<4\text{-}\mu\text{m}$ fraction. We thus cannot rule out an effect of grain size sorting on ${}^{230}\text{Th}$ -normalized MARs during periods of extreme focusing ($\sim 90\%$ of sediments deriving from lateral advection). This effect would be

broadly consistent with the hypothesis of Lyle et al. (2005), in that it would lead to underestimation of rain rates in focused sediments, but the magnitude of the effect is much smaller than that hypothesized by Lyle et al.: comparison of ^{230}Th -normalized MARs between sites and with ^3He -normalized MARs suggests that grain size fractionation during transport results in an underestimation of MARs by at most 40%, despite the ten-fold focusing of laterally advected sediment. Moreover, the fact that glacial ^{230}Th -normalized MARs at GGC39 are similar to those at sites 51GGC and CH88-11 despite the different locations (1790 to 3337 m water depth) and very large differences in lateral advection between the 3 sites (age model MARs ranging from <4 to $>70\text{ g cm}^{-2}\text{ kyr}^{-1}$) (Fig. 2) suggests that it is the glacial ^{230}Th -normalized MARs at GGC40, the site with less focusing, that are instead anomalous.

Glacial ^{230}Th - and ^3He -normalized MARs are a factor of 2–3 greater than Holocene MARs in each core, raising the question of whether this difference is an artifact of increased glacial sediment advection or whether it represents a true Holocene–glacial difference in vertical rain rates. Sand flux data calculated using the age model for each core provide an independent indication of relative changes in vertical rain rates; as sand is generally not able to be transported by bottom currents, sand accumulation is interpreted to represent local water column inputs (Keigwin and Schlegel, 2002). Sand fluxes are a factor of 2–2.5 higher in the glacial than in the Holocene in both cores, consistent with the relative change in ^{230}Th - and ^3He -normalized MARs (Fig. 4). The glacial–Holocene change in rain rates is also consistent with ^{230}Th -normalized MARs from core 51GGC (Gutjahr et al., 2008), a core with an opposite pattern of glacial–Holocene lateral advection changes (Fig. 2). Additionally, several previous studies have indicated increased rain rates in the equatorial and North Atlantic during the last glacial period (Bacon, 1984; Broecker et al., 1958; Francois and Bacon, 1994; Luo et al., 2001; McManus et al., 1998, 2004; Thomson et al., 1999), due in part to increased riverine inputs to the continental slope during this time of low sea levels (Francois and Bacon, 1991). The agreement both with sand MAR data from within the cores and with data from sites with different lateral advection histories offers an important consistency check on CFP-normalized MARs and indicates that despite the large Holocene–glacial difference in sediment advection, normalization to $^{230}\text{Th}_{\text{xs}}$ and $^3\text{He}_{\text{ET}}$ produces internally consistent MAR estimates in both time periods.

On a more basic level, it is important to note that the hypothesis that ^{230}Th -normalized MARs may be biased by advection of $^{230}\text{Th}_{\text{xs}}$ -enriched fine particles predicts that ^{230}Th -normalized MARs should be low during periods of high lateral advection (Lyle et al., 2005). We instead observe a substantial increase in ^{230}Th - and ^3He -normalized MARs during the period of maximum lateral advection in both cores.

4.4. Grain size distribution of $^{230}\text{Th}_{\text{xs}}$ and $^3\text{He}_{\text{ET}}$

Concentrations of $^{230}\text{Th}_{\text{xs}}$ are higher in the $<4\text{-}\mu\text{m}$ fraction than in either the bulk sediment or in the 4- to $20\text{-}\mu\text{m}$ fraction (Fig. 5A). The magnitude of this difference in Holocene samples, a factor of 2 between the $<4\text{-}\mu\text{m}$ and the 4- to $20\text{-}\mu\text{m}$ fractions, is consistent with the findings of Anderson et al. (1983a) in the Panama Basin, Thomson et al. (1993) in the northeast Atlantic, and Kretschmer et al. (2010) in carbonate-rich Walvis Ridge sediments. $^{230}\text{Th}_{\text{xs}}$ concentration differences are much greater in glacial sediments; though only $<4\text{ }\mu\text{m}$ and bulk samples were analyzed, the low bulk $^{230}\text{Th}_{\text{xs}}$ concentrations in glacial sediments require that the $>4\text{-}\mu\text{m}$ fractions of these sediments have $^{230}\text{Th}_{\text{xs}}$ concentrations that average a factor of ~ 10 lower than in the $<4\text{-}\mu\text{m}$ fraction. This difference is similar to that found in opal-rich sediments by Kretschmer et al. (2010).

The enrichment of fine material in advected sediments, combined with the fact that $^{230}\text{Th}_{\text{xs}}$ is concentrated in $<4\text{-}\mu\text{m}$ grains, suggests that ^{230}Th -normalized MARs should be sensitive to sediment

redistribution. We find, however, that redistribution has minimal effects on total sedimentary $^{230}\text{Th}_{\text{xs}}$, as ^{230}Th -normalization produces reasonable MAR estimates even in settings where the supply of advected material exceeds the local rain rate by a factor of ~ 10 ; similarly, Thomson et al. (1999) demonstrated that ^{230}Th -normalized MARs in Iberian margin sites with focusing factors of 3–4 were identical to those in a nearby open-ocean site with minimal focusing.

One explanation for this seeming discrepancy is that though differences in ^{230}Th (and ^3He) concentrations between clay-sized and coarser grains may be large, fractionation during transport is relatively slight. Studies such as the present work are able to isolate clay-sized grains using a chemical dispersant and purified water, but in seawater the behavior of particles smaller than $\sim 10\text{ }\mu\text{m}$ is strongly affected by cohesive forces (McCave and Hall, 2006). Studies of sediment deposition have found that grains smaller than $\sim 10\text{--}20\text{ }\mu\text{m}$ are dominantly deposited as larger aggregates rather than as single grains (Curran et al., 2004; Kranck and Milligan, 1991), meaning that $1\text{-}\mu\text{m}$ grains and $10\text{-}\mu\text{m}$ grains typically have the same effective settling velocity. Once deposited, $<10\text{-}\mu\text{m}$ grains have critical erosion thresholds (i.e., shear stresses necessary for resuspension) similar to much coarser grains due to cohesive forces (McCave and Hall, 2006 and references therein). Accordingly, Kretschmer et al. (2010) were unable to separate $<2\text{-}\mu\text{m}$ grains when sediment samples were suspended in seawater due to flocculation of the fine grains. Lateral advection thus may not substantially fractionate 10- to $20\text{-}\mu\text{m}$ grains from smaller particles, and so the differences observed in this study between $^{230}\text{Th}_{\text{xs}}$ concentrations in different size fractions may have little effect on the $^{230}\text{Th}_{\text{xs}}$ inventory in cores containing advected material. Consistent with this hypothesis, Kretschmer et al. (2010) found much smaller differences in $^{230}\text{Th}_{\text{xs}}$ concentrations across grain sizes when size separations were performed in natural seawater instead of purified water, likely due to the presence of aggregates containing fine grains within the coarser fractions: $^{230}\text{Th}_{\text{xs}}$ concentrations were only a factor of 1.2–1.9 higher in $<10\text{-}\mu\text{m}$ grains than in 10- to $20\text{-}\mu\text{m}$ grains, and only a factor of <1.5 higher in 10- to $20\text{-}\mu\text{m}$ grains than in 20- to $63\text{-}\mu\text{m}$ grains. The small magnitude of these differences substantially reduces the possibility that lateral advection will bias ^{230}Th -normalized MAR estimates (Francois et al., 2007).

We also note that the sensitivity of ^{230}Th -normalized MARs at a site to additions of size-fractionated laterally advected material depends on the grain size distribution of locally derived sediments at the site. In most deep sea sediments, the grain size distribution is strongly skewed toward $<20\text{-}\mu\text{m}$ grains. Additions of clay- and silt-sized grains by lateral advection thus have little effect on the overall grain size distribution and on the abundance of $^{230}\text{Th}_{\text{xs}}$ -enriched fine grains, making it unlikely that ^{230}Th -normalized MARs will be changed by more than a few tens of percent by sediment focusing.

The grain size distribution of $^3\text{He}_{\text{ET}}$ reflects the grain size distribution of He-bearing IDPs. Concentrations of $^3\text{He}_{\text{ET}}$ in each size fraction are not the best indicator of this distribution, as concentrations are strongly influenced by differences in sediment supply between size fractions. We therefore focus on the inventory of $^3\text{He}_{\text{ET}}$ in each size fraction (the product of the concentration of $^3\text{He}_{\text{ET}}$ in a size fraction by the percent of the total sediment within that size fraction) rather than the concentration. Like $^{230}\text{Th}_{\text{xs}}$ concentrations, $^3\text{He}_{\text{ET}}$ inventories are highest in fine-grained sediments, as on average $>90\%$ of $^3\text{He}_{\text{ET}}$ is in $<20\text{-}\mu\text{m}$ grains (Fig. 5b). This result is in general agreement with previous studies indicating that ^3He -retentive IDPs are dominantly in fine silt- and clay-sized grains (Brook et al., 2009; Farley et al., 1997). We do not find evidence for a peak in the distribution of $^3\text{He}_{\text{ET}}$ in the 5- to $10\text{-}\mu\text{m}$ range as recently observed in an Antarctic ice sample (Brook et al., 2009), although this difference could reflect incomplete separation of $<4\text{ }\mu\text{m}$ material from the 4- to $20\text{-}\mu\text{m}$ fraction in this study.

As both Holocene and glacial sediments in GGC39 contain laterally advected sediments likely to be enriched in fine grains, our data may overestimate $^3\text{He}_{\text{ET}}$ inventories in the fine fraction of the sediment.

Based upon the difference between ^{230}Th -normalized MARs and age model MARs, laterally advected material makes up approximately 2/3 of GGC39 sediment in the Holocene. Assuming that only $<20\text{-}\mu\text{m}$ grains are advected, we calculate that $\sim 70\%$ of $^3\text{He}_{\text{ET}}$ is in $<20\text{-}\mu\text{m}$ grains.

5. Conclusions

We find that normalization to $^{230}\text{Th}_{\text{xs}}$ and $^3\text{He}_{\text{ET}}$ produces internally consistent estimates of sedimentary mass accumulation rates even in settings where lateral sediment inputs exceed local rain rates by a factor of ~ 10 . Vertical rain rates estimated by ^{230}Th - and ^3He -normalized MARs reproduce Holocene–glacial rain rate changes indicated by sand MARs despite large spatial and temporal differences in lateral advection. Holocene ^{230}Th - and ^3He -normalized MARs indicate equal rain rates in two cores separated by only 10 km but with lateral advection rates differing by a factor of 2. ^3He -normalized MARs are also not significantly different between sites in the glacial, when both sites experienced high but differing rates of lateral advection. ^{230}Th -normalized MARs differ between the sites by 40% in the glacial, requiring further investigation. Comparison of our $^{230}\text{Th}_{\text{xs}}$ data to those from two other Blake Ridge sites suggests that ^{230}Th -normalized MARs in GGC39 – the site experiencing the highest inputs of laterally advected sediments – are reasonable, while $^{230}\text{Th}_{\text{xs}}$ concentrations at GGC40 are anomalously low between 17.5 and 20 ka, producing high ^{230}Th -normalized MARs. The overall consistency of both $^3\text{He}_{\text{ET}}$ and $^{230}\text{Th}_{\text{xs}}$ concentrations suggests that both constant-flux proxies are able to quantify rates of lateral sediment advection in drift deposits. In continental margin settings such as the Blake Ridge, knowledge of detrital $^{230}\text{Th}/^{232}\text{Th}$ and $^3\text{He}/^4\text{He}$ ratios is required for precise data; further work is needed to improve methods of constraining detrital $^3\text{He}/^4\text{He}$ in drift deposits.

Measurements of $^{230}\text{Th}_{\text{xs}}$ and $^3\text{He}_{\text{ET}}$ in grain size fractions indicates that both are concentrated in fine particles ($<4\text{ }\mu\text{m}$ for $^{230}\text{Th}_{\text{xs}}$ and $<20\text{ }\mu\text{m}$ for $^3\text{He}_{\text{ET}}$); however, bulk concentrations of both constant-flux proxies appear to be only minimally affected by lateral sediment advection. We suggest that the limited impacts of lateral advection may result from the cohesive behavior of fine particles in marine settings, which limits fractionation of $<4\text{-}\mu\text{m}$ grains from coarser grains and thus limits differences in $^{230}\text{Th}_{\text{xs}}$ concentrations and $^3\text{He}_{\text{ET}}$ inventories between vertical rain and laterally advected sediments. The impacts of lateral advection may be further minimized due to the high proportions of $<20\text{-}\mu\text{m}$ grains in both vertical rain and laterally advected sediments in most of the world's oceans. Overall, our results do not support the suggestion that preferential transport of fine grains during lateral advection substantially biases ^{230}Th - and ^3He -based MAR estimates.

Supplementary materials related to this article can be found online at [doi:10.1016/j.epsl.2010.08.029](https://doi.org/10.1016/j.epsl.2010.08.029).

Acknowledgements

The authors thank Robert F. Anderson, Maureen Auro, Linda Baker, Wallace Broecker, Susan Brown-Leger, Tom Cronin, Helena Evans, Lloyd Keigwin, Tim Kenna, Joanne Goudreau, Kais J. Mohamed, Summer Praetorius, Laura Robinson, and Roseanne Schwartz, all of whom contributed either to data collection or interpretation. Three anonymous reviewers offered comments that improved the manuscript. We also wish to acknowledge support from NSF (OCE-0550763; F.M. and J.F.M.), the NSF Graduate Research Fellowship and GK-12 programs (D.M.) and the Comer Science and Education Foundation (D.M., J.F.M. and G.W.).

References

Anderson, R.F., Bacon, M.P., Brewer, P.G., 1983a. Removal of ^{230}Th and ^{231}Pa at ocean margins. *Earth Planet. Sci. Lett.* 66, 73–90.
 Anderson, R.F., Bacon, M.P., Brewer, P.G., 1983b. Removal of ^{230}Th and ^{231}Pa from the open ocean. *Earth Planet. Sci. Lett.* 62, 7–23.

Anderson, R.F., Fleisher, M.Q., Biscaye, P.E., Kumar, N., Dittrich, B., Kubik, P., Suter, M., 1994. Anomalous boundary scavenging in the Middle Atlantic Bight: evidence from ^{230}Th , ^{231}Pa , ^{10}Be and ^{210}Pb . *Deep Sea Res.* 41, 537–561.
 Anderson, R.F., Fleisher, M.Q., Lao, Y., Winckler, G., 2008. Modern CaCO_3 preservation in equatorial Pacific sediments in the context of late-Pleistocene glacial cycles. *Mar. Chem.* 111, 30–46.
 Bacon, M.P., 1984. Glacial to interglacial changes in carbonate and clay sedimentation in the Atlantic Ocean estimated from ^{230}Th measurements. *Chem. Geol.* 46, 97–111.
 Biscaye, P.E., Anderson, R.F., 1994. Fluxes of particulate matter on the slope of the southern Middle Atlantic Bight—SEEP II. *Deep Sea Res.* 41, 459–509.
 Broecker, W.S., 2008. Excess sediment ^{230}Th : transport along the sea floor or enhanced water column scavenging? *Glob. Biogeochem. Cycles* 22, GB1006.
 Broecker, W.S., Turekian, K.K., Heezen, B.C., 1958. The relation of deep sea sedimentation rates to variations in climate. *Am. J. Sci.* 256, 503–517.
 Brook, E.J., Kurz, M.D., Curtice, J., Cowburn, S., 2000. Accretion of interplanetary dust in polar ice. *Geophys. Res. Lett.* 27, 3145–3148.
 Brook, E.J., Kurz, M.D., Curtice, J., 2009. Flux and size fractionation of ^3He in interplanetary dust from Antarctic ice core samples. *Earth Planet. Sci. Lett.* 286, 565–569.
 Chase, Z., Anderson, R.F., Fleisher, M.Q., Kubik, P.W., 2002. The influence of particle composition and particle flux on scavenging of Th, Pa and Be in the ocean. *Earth Planet. Sci. Lett.* 204, 215–229.
 Cheng, H., Edwards, R.L., Hoff, J., Gallup, C.D., Richards, D.A., Asmerom, Y., 2000. The half-lives of uranium-234 and thorium-230. *Chem. Geol.* 169, 17–33.
 Choi, M.S., Francois, R., Sims, K., Bacon, M.P., Brown-Leger, S., Fleer, A.P., Ball, L., Schneider, D., Pichat, S., 2001. Rapid determination of ^{230}Th and ^{231}Pa in seawater by desolvated micro-nebulization inductively coupled plasma magnetic sector mass spectrometry. *Mar. Chem.* 76, 99–112.
 Curran, K.J., Hill, P.S., Schell, T.M., Milligan, T.G., Piper, D.J.W., 2004. Inferring the mass fraction of floc-deposited mud: application to fine-grained turbidites. *Sedimentology* 51, 927–944.
 Evans, H.K., Hall, I.R., 2008. Deepwater circulation on Blake Outer Ridge (western North Atlantic) during the Holocene, Younger Dryas, and Last Glacial Maximum. *Geochem. Geophys. Geosyst.* 9, Q03023. doi:10.1029/2007GC001771.
 Farley, K.A., Patterson, D.B., 1995. A 100-kyr periodicity in the flux of extraterrestrial ^3He to the sea floor. *Nature* 378, 600–603.
 Farley, K.A., Love, S.G., Patterson, D.B., 1997. Atmospheric entry heating and helium retentivity of interplanetary dust particles. *Geochim. Cosmochim. Acta* 61, 2309–2316.
 Fourre, E., 2004. A 475 kyr record of extraterrestrial ^3He and ^{230}Th in North Atlantic sediments: caveats to derive MAR from these tracers. *Eos Trans. AGU 85 Fall Meet. Suppl.*, Abstract.
 Francois, R., Bacon, M.P., 1991. Variations in terrigenous input into the deep equatorial Atlantic during the past 24,000 years. *Science* 251, 1473–1476.
 Francois, R., Bacon, M.P., 1994. Heinrich events in the North Atlantic: radiochemical evidence. *Deep Sea Res.* 41, 315–334.
 Francois, R., Bacon, M.P., Suman, D.O., 1990. Thorium 230 profiling in deep-sea sediments: high-resolution records of flux and dissolution of carbonate in the equatorial Atlantic during the last 24,000 years. *Paleoceanography* 5, 761–787.
 Francois, R., Bacon, M.P., Altabet, M.A., Labeyrie, L.D., 1993. Glacial-interglacial changes in sediment rain rate in the SW Indian sector of sub-Antarctic waters as recorded by ^{230}Th , ^{231}Pa , U, and $\delta^{15}\text{N}$. *Paleoceanography* 8, 611–629.
 Francois, R., Frank, M., van der Loeff, M.M.R., Bacon, M.P., 2004. ^{230}Th normalization: an essential tool for interpreting sedimentary fluxes during the late Quaternary. *Paleoceanography* 19, PA1018.
 Francois, R., Frank, M., Rutgers van der Loeff, M., Bacon, M.P., Geibert, W., Kienast, S., Anderson, R.F., Bradtmiller, L., Chase, Z., Henderson, G., Marcantonio, F., Allen, S.E., 2007. Comment on “Do geochemical estimates of sediment focusing pass the sediment test in the equatorial Pacific?” by M. Lyle et al. *Paleoceanography* 22, PA1216. doi:10.1029/2005PA001235.
 Gutjahr, M., Frank, M., Stirling, C.H., Keigwin, L.D., Halliday, A.N., 2008. Tracing the Nd isotope evolution of North Atlantic Deep and Intermediate Waters in the western North Atlantic since the Last Glacial Maximum from Blake Ridge sediments. *Earth Planet. Sci. Lett.* 266, 61–77.
 Heezen, B.C., Hollister, C.D., Ruddiman, W.F., 1966. Shaping of the continental rise by deep geostrophic contour currents. *Science* 152, 502–508.
 Henderson, G.M., Anderson, R.F., 2003. The U-series toolbox for paleoceanography. *Rev. Mineral. Petrol.* 52, 493–531.
 Henderson, G.M., Heinze, C., Anderson, R.F., Winguth, A.M.E., 1999. Global distribution of the Th-230 flux to ocean sediments constrained by GCM modelling. *Deep Sea Res.* 46, 1861–1893.
 Higgins, S.M., Anderson, R.F., Marcantonio, F., Schlosser, P., Stute, M., 2002. Sediment focusing creates 100-ka cycles in interplanetary dust accumulation on the Ontong Java Plateau. *Earth Planet. Sci. Lett.* 203, 383–397.
 Keigwin, L.D., Schlegel, M.A., 2002. Ocean ventilation and sedimentation since the glacial maximum at 3 km in the western North Atlantic. *Geochem. Geophys. Geosyst.* 3, 1034.
 Kienast, S.S., Kienast, M., Mix, A.C., Calvert, S.E., Francois, R., 2007. Thorium-230 normalized particle flux and sediment focusing in the Panama Basin region during the last 30,000 years. *Paleoceanography* 22, PA2213. doi:10.1029/2006PA001357.
 Kranck, K., Milligan, T.G., 1991. Grain size in oceanography. In: Syvitski, J.P.M. (Ed.), Principles, Methods, and Application of Particle Size Analysis. Cambridge Univ. Press, New York, pp. 332–345.
 Kretschmer, S., Geibert, W., Rutgers van der Loeff, M.M., Mollenhauer, G., 2010. Grain size effects on $^{230}\text{Th}_{\text{xs}}$ inventories in opal-rich and carbonate-rich marine sediments. *Earth Planet. Sci. Lett.* 294, 131–142.
 Long, A., Rippeteau, B., 1974. Testing contemporaneity and averaging radiocarbon dates. *Am. Antiq.* 39, 205–215.

- Loubere, P., Mekik, F., Francois, R., Pichat, S., 2004. Export fluxes of calcite in the eastern equatorial Pacific from the Last Glacial Maximum to present. *Paleoceanography* 19, PA2018. doi:10.1029/2003PA000986.
- Luo, S.D., Ku, T.L., Wang, L., Southon, J.R., Lund, S.P., Schwartz, M., 2001. Al-26, Be-10 and U-Th isotopes in Blake Outer Ridge sediments: implications for past changes in boundary scavenging. *Earth Planet. Sci. Lett.* 185, 135–147.
- Lyle, M., Mitchell, N., Piasias, N., Mix, A., Martinez, J.J., Paytan, A., 2005. Do geochemical estimates of sediment focusing pass the sediment test in the equatorial Pacific? *Paleoceanography* 20, PA1005.
- Mamyrin, B.A., Tolstikhin, I.N., 1984. Helium Isotopes in Nature. Elsevier.
- Marcantonio, F., Kumar, N., Stute, M., Anderson, R.F., Seidl, M.A., Schlosser, P., Mix, A., 1995. Comparative study of accumulation rates derived by He and Th isotope analysis of marine sediments. *Earth Planet. Sci. Lett.* 133, 549–555.
- Marcantonio, F., Anderson, R.F., Stute, M., Kumar, N., Schlosser, P., Mix, A., 1996. Extraterrestrial ^3He as a tracer of marine sediment transport and accumulation. *Nature* 383, 705–707.
- Marcantonio, F., Higgins, S., Anderson, R.F., Stute, M., Schlosser, P., Rasbury, E.T., 1998. Terrestrial helium in deep-sea sediments. *Geochim. Cosmochim. Acta* 62, 1535–1543.
- Marcantonio, F., Anderson, R.F., Higgins, S., Stute, M., Schlosser, P., Kubik, P., 2001. Sediment focusing in the central equatorial Pacific Ocean. *Paleoceanography* 16, 260–267.
- McCave, I.N., Hall, I.R., 2006. Size sorting in marine muds: processes, pitfalls, and prospects for paleoflow-speed proxies. *Geochem. Geophys. Geosyst.* 7, Q10N05.
- McManus, J.F., Anderson, R.F., Broecker, W.S., Fleisher, M.Q., Higgins, S.M., 1998. Radiometrically determined sedimentary fluxes in the sub-polar North Atlantic during the last 140,000 years. *Earth Planet. Sci. Lett.* 155, 29–43.
- McManus, J.F., Francois, R., Gherardi, J.M., Kelgwin, L., Brown-Leger, S., 2004. Collapse and rapid resumption of Atlantic meridional circulation linked to deglacial climate changes. *Nature* 428, 834–837.
- Mollenhauer, G., McManus, J.F., Benthien, A., Muller, P.J., Eglinton, T.J., 2006. Rapid lateral particle transport in the Argentine Basin: molecular ^{14}C and $^{230}\text{Th}_{(xs)}$ evidence. *Deep Sea Res.* 53, 1224–1243.
- Mukhopadhyay, S., Farley, K.A., 2006. New insights into the carrier phase(s) of extraterrestrial ^3He in geologically old sediments. *Geochim. Cosmochim. Acta* 70, 5061–5073.
- Nier, A.O., Schlutter, D.J., 1990. Helium and neon in stratospheric particles. *Meteoritics* 25, 263–267.
- Paytan, A., Lyle, M., Mix, A., Chase, Z., 2004. Climatically driven changes in oceanic processes throughout the equatorial Pacific. *Paleoceanography* 19, PA4017.
- Robinson, L.F., Belshaw, N.S., Henderson, G.M., 2004. U and Th concentrations and isotope ratios in modern carbonates and waters from the Bahamas. *Geochim. Cosmochim. Acta* 68, 1777–1789.
- Schlegel, M.A., 1998. Paleoclimatological variability on a millennial scale: a high resolution record of the latest deglaciation from the Blake Outer Ridge, western North Atlantic. Masters thesis, Massachusetts Institute of Technology and Woods Hole Oceanographic Institution.
- Siddall, M., Anderson, R.F., Winckler, G., Henderson, G.M., Bradtmiller, L.I., McGee, D., Franzese, A., Stocker, T.F., Muller, S.A., 2008. Modeling the particle flux effect on distribution of Th-230 in the equatorial Pacific. *Paleoceanography* 23, PA2208. doi:10.1029/2007PA001556.
- Solomon, D.K., Hunt, A., Poreda, R.J., 1996. Source of radiogenic helium 4 in shallow aquifers: implications for dating young groundwater. *Water Resour. Res.* 32, 1805–1813.
- Stahr, F.R., Sanford, T.B., 1999. Transport and bottom boundary layer observations of the North Atlantic Deep Western Boundary Current at the Blake Outer Ridge. *Deep Sea Res.* 46, 205–243.
- Suman, D.O., Bacon, M.P., 1989. Variations in Holocene sedimentation in the North American Basin determined from ^{230}Th measurements. *Deep Sea Res.* 36, 869–878.
- Thomson, J., Colley, S., Anderson, R., Cook, G.T., MacKenzie, A.B., Harkness, D.D., 1993. Holocene sediment fluxes in the northeast Atlantic from $^{230}\text{Th}_{\text{excess}}$ and radiocarbon measurements. *Paleoceanography* 8 (5), 631–650.
- Thomson, J., Nixon, S., Summerhayes, C.P., Schonfeld, J., Zahn, R., Grootes, P., 1999. Implications for sedimentation changes on the Iberian margin over the last two glacial/interglacial transitions from $^{230}\text{Th}_{\text{excess}(0)}$ systematics. *Earth Planet. Sci. Lett.* 165, 255–270.
- Thomson, J., Green, D.R.H., van Calsteren, P., Richter, T.O., van Weering, T.C.E., 2006. Holocene sediment deposition on a NE Atlantic transect including Feni Drift quantified by radiocarbon and $^{230}\text{Th}_{\text{excess}}$ methods. *Earth Planet. Sci. Lett.* 242, 170–185.
- Tolstikhin, I., Lehmann, B.E., Loosli, H.H., Gauthier, A., 1996. Helium and argon isotopes in rocks, minerals, and related groundwaters: a case study in northern Switzerland. *Geochim. Cosmochim. Acta* 60, 1497–1514.
- Wadell, H., 1932. Volume, shape and roundness of rock particles. *J. Geol.* 40, 443–451.
- Wadell, H., 1934. Some new sedimentation formulas. *J. Appl. Phys.* 5, 281–291.
- Winckler, G., Fischer, H., 2006. 30,000 years of cosmic dust in Antarctic ice. *Science* 313, 491.
- Winckler, G., Anderson, R.F., Stute, M., Schlosser, P., 2004. Does interplanetary dust control 100 kyr glacial cycles? *Quat. Sci. Rev.* 23, 1873–1878.